A Low-cost Small-sized Eddy Current Displacement Sensor

Qian WANG*, Hongkun CHEN*, Zhengzhang YAN* and Jiahao CHEN*
* School of Information Science and Technology, ShanghaiTech University, China
chenjh2@shanghaitech.edu.cn

Abstract
This paper designs small-sized printed circuit board (PCB) coils along with commercial inductance-to-digital converter (LDC) from Texas Instruments, and evaluates its potential for space limited bearingless motor applications, e.g., artificial hearts. For instance, the rarial displacement of the rotor, measured in x- and y-components, can be captured by two PCB coils with one LDC1612 chip. The measurement range and resolution of the sensor are measured in experiments, and variants of PCB coil shapes are further considered and compared.

Keywords : printed circuit board coils, displacement sensors, bearingless motors.

1. Introduction

The displacement sensor provides high bandwidth feedback signal for active control of rotor displacement in magentically levitated system. There are various types of displacement sensors, including capacitive, Hall-effect, and eddy current sensors. Capacitive displacement sensors are usually expensive and highly sensitive to air gap media [1]. Hall-effect displacement sensors require an excitation source and indirectly measure displacement by measuring the strength of the magnetic field [2]. Among the three, eddy current displacement sensors have been widely used in magnetic levitation motor systems [3–5].

Existing eddy current displacement sensors in litrerature is bulky in design [6]. A typical example is shown in Fig. 1. The outer sensor diameter of the sensor is about 100 mm, which is not suited for space-constrained applicaiton. On the other hand, the small-sized eddy current displacement sensor avalilable in the market is expensive, e.g., priced at $600 [7]. In this paper, a low-cost (all configurations add up to only a few tens of dollars), high-accuracy, and compact noncontact eddy current displacement sensor design based on printed-circuit board (PCB) coils and commercial inductance-to-digital converter (LDC1612) from Texas Instruments (TI) is proposed.

Given the fact that integrating multi-coil array eddy current sensors has emerged as a research hotspot due to their capability to simultaneously decouple axial and radial displacements [8, 9]. This paper focuses on in-depth optimization of a high-precision single-point eddy current displacement sensor. By investigating the influence of probe coil geometry on sensor performance and quantifying resolution characteristics at varying distances, this work provides a moduilarized components for multi-coil array eddy current displacement sensors.

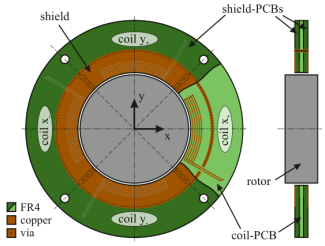

Fig. 1 PCB integrated radial eddy current sensor design [10].

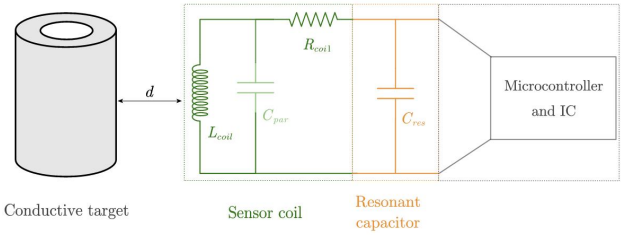

Fig. 2 Working principle of the eddy current displacement sensor.

2. Design Process for the Proposed Displacement Sensor

The PCB coil can be equivalently modeled as an electromagnet. When an alternating current flows through PCB coil,

an alternating magnetic field (AC magnetic field) is generated around it. If a conductive material, such as a metal object, is brought near this changing magnetic field, circulating currents, commonly known as eddy currents, will be induced on the surface of the conductive target.

The changing eddy current, in turn, generates an induced magnetic field in the opposite direction of the original magnetic field. This effect can be equivalently regarded as a set of coupled inductors in circuit, where the PCB coil acts as the primary inductor and the eddy currents in the target conductor represent the secondary inductor. The coupling between the primary and secondary inductors is a function of the resistivity, size, shape, and distance of the PCB coil and the target conductor. When the intrinsic parameters (such as resistivity, size, and shape) are fixed, the only factor that influences coupling strength is the distance d between the PCB coil and the target conductor. Fig. 2 shows a simplified model of the PCB coil and the target conductor with respect to their distance d. In this model, L_{coil}, R_{coil}, and C_{par} represent the inductance, resistance, and parasitic capacitance of the PCB coil, respectively. Meanwhile, C_{res} denotes the capacitance connected to the PCB coil, forming a resonator.

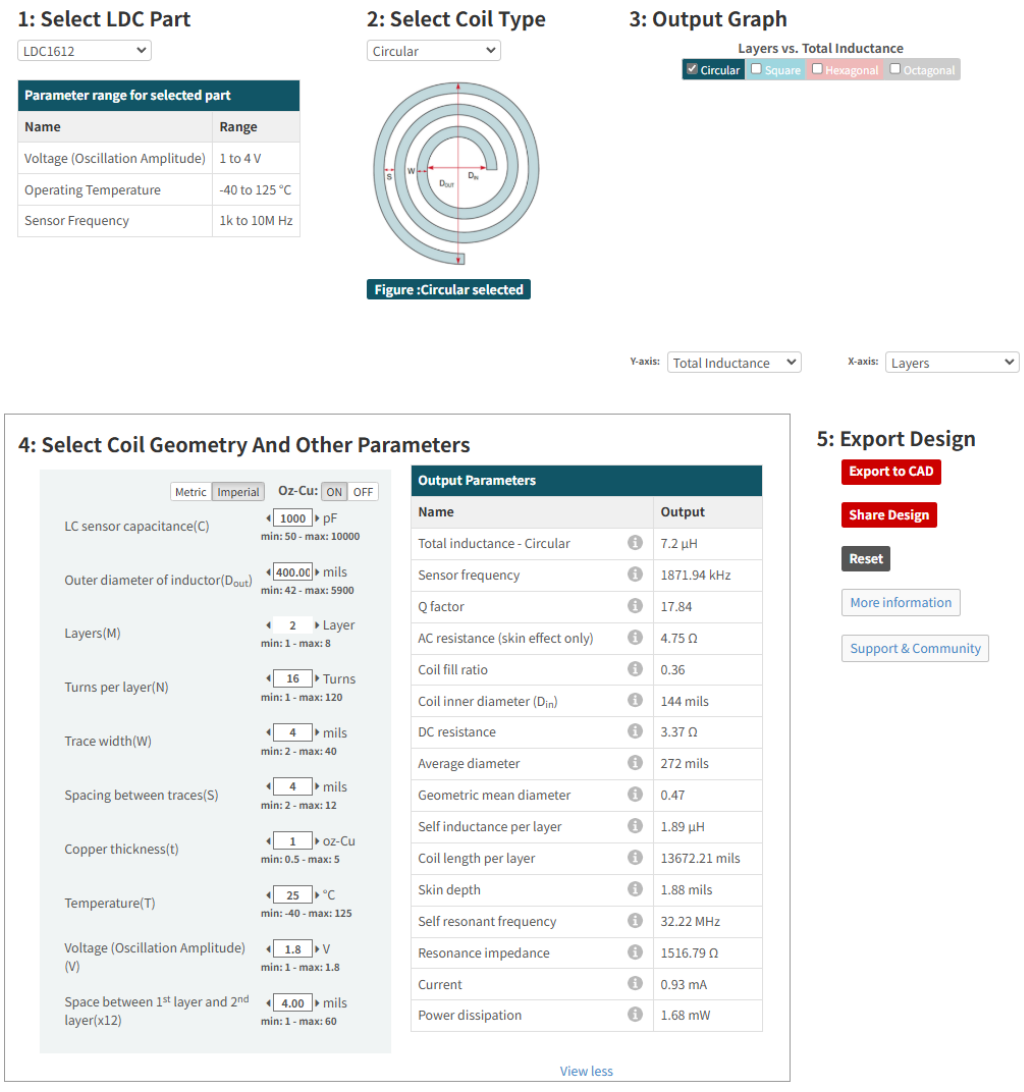

Fig. 3 Coil designer provided by TI [11].

The PCB coil calculator provided by TI can be directly utilized for sensor parameter design [11], as shown in Fig. 3.

Step one is to select the LDC part. To convert the coupled inductance into a digital signal, the inductance-to-digital converter [12] is used, which is an integrated circuit (IC) developed by *TI*. The microcontroller communicates with LDC1612 via the I2C protocol, enabling real-time transmission of the digital signal to the computer. The LDC1612 series can use up to two PCB coils, while the LDC1614 series can use up to four PCB coils.

Step two is to select coil type, we can choose circular, square, hexagonal and octagonal, Each coil configuration is defined by four key geometric parameters: inter turn gap (s), conductor line width (w), outer contour dimensions (D_{OUT},

representing equivalent edge length in square coils), and inner aperture (D_{IN}). The parameters s, w and D_{OUT} can be dynamically adjusted in the step four.

Step three is to choose layers, we can choose from one layer to eight layers, and the total inductance would increase if we choose a higher layer number, which means a more stable PCB coil.

Step four is to determine the geometric parameters of the coil, including trace width, turns per layer, spacing between traces, and spacing between layers. At the same time, some other circuit related parameters can also be determined, including copper thickness and LC sensor capacitance (which is the resonant capacitor as mentioned previously in Fig. 2). When the above parameters are determined, the coil desinger can automatically generate PCB coils corresponding to these parameters, while providing some output parameters, including total inductance, sensor frequency, Q factor, and self resonant frequency.

It is worth noting that if in practical applications two PCB coils are too close together (with a distance less than the coil diameter), then these two coils should choose different frequencies to avoid interference.

Upon completion of the design, the PCB layout schematic of the PCB coil can be exported. Subsequently, open-source and free PCB design software can be employed for PCB editing. Based on the geometry of the target bearingless motor (BLM) stator, the external contour of the PCB coil was customized, resulting in a final design compatible with a circular motor housing.

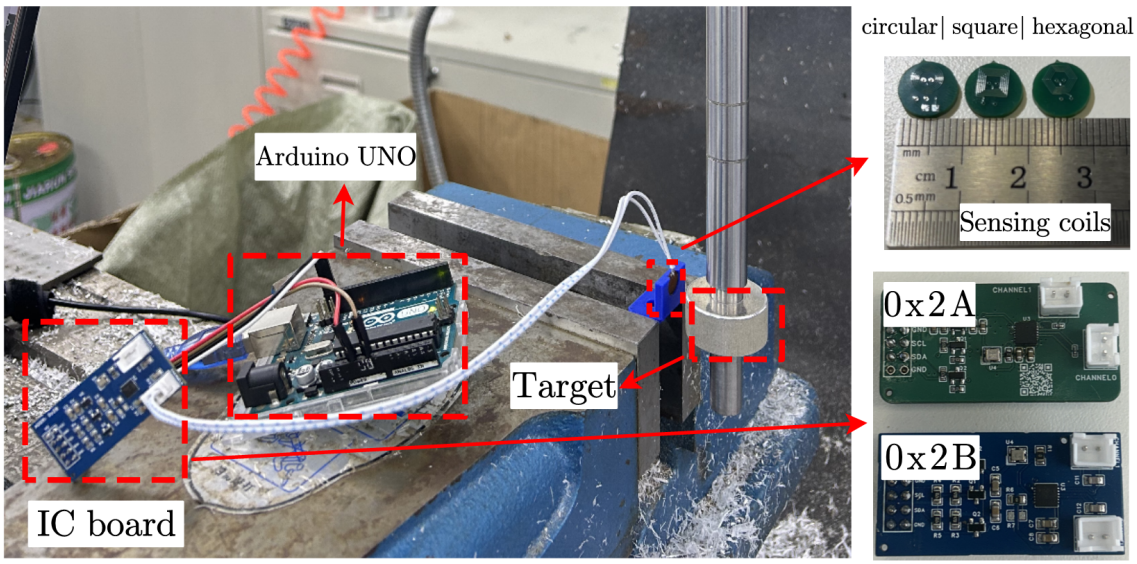

Fig. 4 Test bench setup on a CNC platform.

3. Experimental Validation Studies

The test bench uses a three-axis milling machine to control the displacement between the sensing target and the PCB coil. The positioning resolution is 5 μm. As illustrated in Fig. 4, the experimental configuration consists of:

- a bearingless motor shaft fixed by the milling head;
- a 6061 aluminum alloy sensing target mounted on the shaft surface;
- the sensor's detection coil rigidly mounted on the milling machine base;
- and LDC1612 inductance-to-digital converter and microcontroller.

The displacement calibration procedure was implemented through axial shaft movement. The calibration commenced with incremental axial advancement of the target conductor toward the PCB coil. When monitored data reached its peak value (corresponding to conductor-coil contact state, indicating zero initial displacement gap), this position was established as the displacement origin. Subsequently, programmed control of the milling machine executed discretized stepwise retraction of the shaft along the axial direction at preset micron-level increments (5 μm), while synchronized acquisition of displacement increments and sensor output values enabled characterization of the sensor's resolution and accuracy performance.

To measure the range of the sensor, perform the following experimental steps:

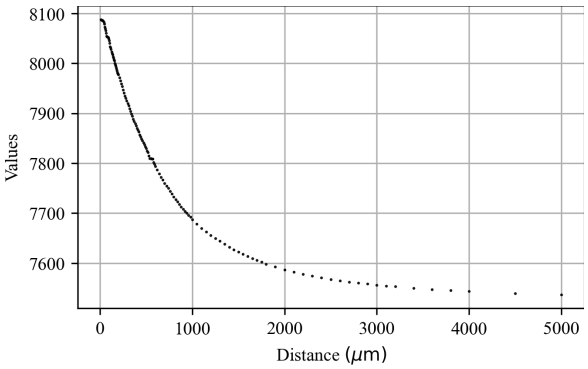

Fig. 5 The values measured by the PCB coil.

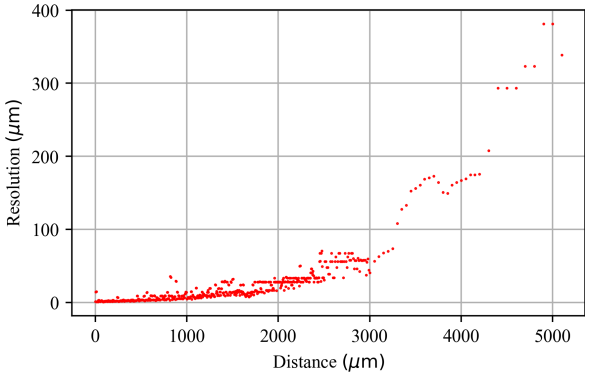

Fig. 6 Resolution curve trend.

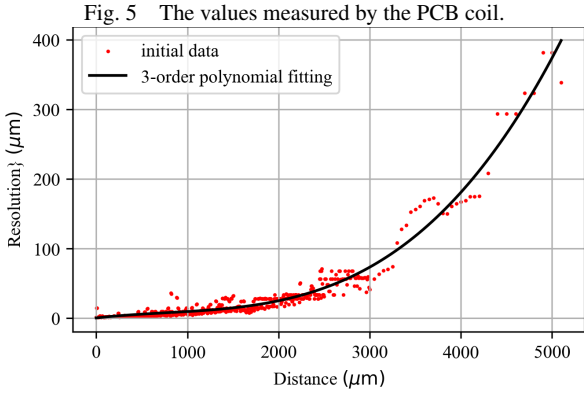

Fig. 7 Resolution fitting curve.

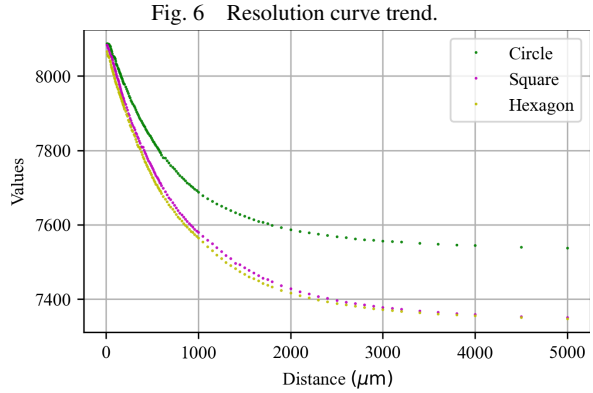

Fig. 8 Measurements by PCB coils of different shapes.

- First, use the milling head to fix the rotor shaft with the target conductor, and fix the PCB coil probe to the milling machine bench;
- Then, adjust the PCB coil to make it parallel to the center of the target conductor surface, and slowly move the machine bench to decide the the initial position corresponding to a zero measurement between the PCB coil and the target conductor;
- Next, record the values of the PCB coil from the zero position, and record the corresponding output values of the PCB coil probe as the milling machine bench moves at a step size of 50 μm. Continue moving the milling machine bench until the values of the PCB coil no longer changes;
- Finally, plot the recoreded data, with the horizontal axis representing the distance between the PCB coil and the target, and the vertical axis representing the inductance digital value of the PCB coil returned by LDC1612, as shown in Fig. 5.

Usually, the effective range of the probe coil detection distance of eddy current displacement sensors is equal to its radius [12]. From Fig. 5 it can be seen that the absolute rate of change measured by the sensor is inversely proportional to the distance of the target conductor. This phenomenon is due to the increased eddy current effect when the distance between the conductor and the coil is shortened, resulting in a significant change in coil impedance.

The diameter of the PCB coil used in this experiment is 5 mm. From Fig. 5, it can be seen that within the range of detection distance from 0 to 5000 μm, that is, within the diameter range of the sensor, the measured values of the sensor have a changing trend. Therefore, it can be concluded that the range of the displacement sensor proposed in this paper can reach the size of the sensor PCB coil diameter, and when the testing distance is within the radius range of the sensor, the values returned by the sensor have a clear changing trend.

As evidenced in Fig. 5, the absolute rate of change in sensor measurements exhibits an inverse relationship with the target conductor distance. This phenomenon arises from enhanced eddy current effects at reduced conductor-to-coil distances, resulting in pronounced coil impedance variations.

In order to better and more accurately calculate the resolution value of the sensor, the displacement adjustment will be made according to the minimum movement unit of the milling machine, which is a distance of 5 μm. Nevertheless, this is still far greater than the optimal resolution value of our sensor. In order to quantify the effective resolution size of the entire range of the sensor, we use derivatives to express this resolution value. The displacement on the x-axis is x, and the return value of the y-axis sensor is y. Therefore, the resolution of the sensor can be expressed as dy/dx.

The displacement sensor's resolution was characterized across discrete operational ranges (0–5 mm). Fig. 6 quantifies resolution distribution, while Fig. 7 presents third-order polynomial fitting curves. Measured resolution demonstrates progressive degradation with increasing displacement. In order to visually illustrate the resolution of the sensor within certain range, the following data is provided (in fact, each specific displacement corresponds to a specific resolution value of the sensor):

- 0-1 mm range: $\leq 10\ \mu$m
- 1-2 mm range: 10-25 μm
- 2-3 mm range: 25-75 μm
- 3-4 mm range: 75-170 μm
- 4-5 mm range: 170-400 μm

Resolution y' versus displacement x follows the empirical relationship:

$$y' = 4.596 \times 10^{-9} x^3 - 1.147 \times 10^{-5} x^2 + 0.01708x - 0.256 \tag{1}$$

It is worth mentioning that when the gap between the displacement sensor and the target conductor is 2.6 mm, the resolution of the sensor can be accurate to within 50 μm.

Inspired by the work in [13], this paper examines and compares the test values obtained from various shapes (circular, square, and hexagonal PCB coils), Fig. 9 shows the different shapes of the PCB coils, and the test values are as illustrated in Fig. 8. Compared to circular PCB coils, square and hexagonal PCB coils have a wider range of variation under the same range. In other words, the latter two have a higher resolution. However, compared to the other two shapes of sensors, the circular PCB coil has a smoother trend of variation and better stability. Therefore, the displacement sensor proposed in this paper can be applied to various shapes, which also meets the requirements of different environments and situations for the shape of the PCB coils.

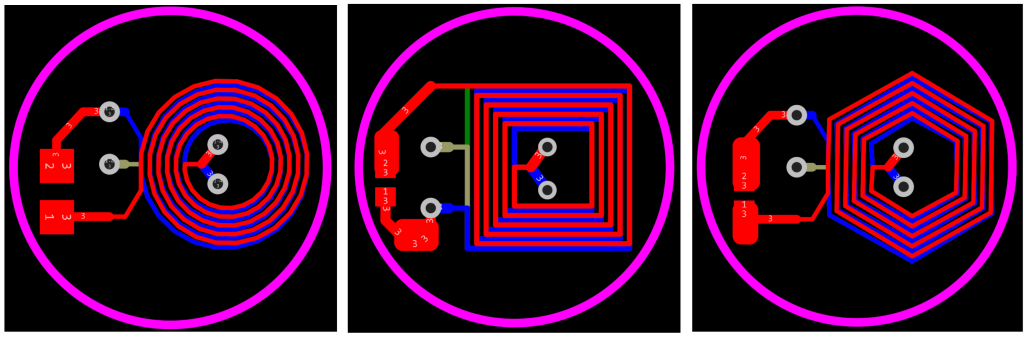

Circular Square Hexagonal

Fig. 9 Variants of different geometric shapes of PCB coils designs.

4. Conclusion

This paper presented a low-cost small-sized displacement sensor. Firstly, the total cost of all components (MCU and sensor prototypes) of the sensor is only a few tens of dollars, and its size and diameter used in bearingless motors are only 5 mm, which can be well applied in space limited magnetic levitation systems. Subsequently, through experimental testing, the range and resolution of the displacement sensor was determinedm, which suggests the measuremnt value is essentially a stochasitc variable. The effective range is the radius of the PCB coil, and its maximum range can reach the diameter of the PCB coil. Finally, the test results of PCB coils with different shapes were compared under similar inductance values and quality factors.

5. Acknowledgment

The authors gratefully acknowledge Kunyong Lv for his essential contribution to experimental data acquisition.

References

[1] E. Maslen, G. Schweitzer, H. Bleuler, M. Cole, P. Keogh, R. Larsonneur, R. Nordmann, Y. Okada, and A. Traxler, *Magnetic Bearings—Theory, Design and Application to Rotating Machinery*, 01 2009.

[2] M. Akrami, E. Jamshidpour, and V. Frick, "Application of hall position sensor in control and position estimation of pmsm - a review," in *2023 IEEE International Conference on Environment and Electrical Engineering and 2023 IEEE Industrial and Commercial Power Systems Europe (EEEIC / ICPS Europe)*, June 2023, pp. 1–6.

[3] J. Passenbrunner, G. Jungmayr, M. Panholzer, S. Silber, and W. Amrhein, "Simulation and optimization of an eddy current position sensor," in *2015 IEEE 11th International Conference on Power Electronics and Drive Systems*, June 2015, pp. 171–176.

[4] M. Noh, W. Gruber, and D. L. Trumper, "Low-cost eddy-current position sensing for bearingless motor suspension control," in *2017 IEEE International Electric Machines and Drives Conference (IEMDC)*, May 2017, pp. 1–6.

[5] P. Peralta, S. Thomas, and Y. Perriard, "Characterization and verification of eddy-current position sensing for magnetic levitation," *IEEE Transactions on Industry Applications*, vol. 57, no. 6, pp. 5796–5805, Nov 2021.

[6] M. Štusák, "Eddy current sensors for magnetic bearings of the textile spinning machines," *Proceedings of ISMB14*, 2014.

[7] AEC,PU-05, https://www.aec-jpn.com/en/products/eddycurrent/en_standardtype/item_005.

[8] R. Yang, Z. He, N. Sugita, and T. Shinshi, "Radial displacement measurement method in bearingless slice motor through eddy current displacement sensors positioned on the underside of the rotor," *IEEE Access*, vol. 12, pp. 26 610–26 625, 2024.

[9] K. Kant and D. L. Trumper, "A 6-dof position sensor for bearingless slice motors," *IEEE Transactions on Industrial Electronics*, vol. 71, no. 4, pp. 4283–4290, April 2024.

[10] D. Wimmer, M. Hutterer, and M. Schrodl, "Design of a pcb integrated eddy current sensor with shield feature for radial rotor displacement measurement," in *Proceedings of ISMB18*, 2023.

[11] Coil Designer, https://webench.ti.com/wb5/LDC/#/spirals.

[12] *LDC1612, LDC1614 Multi-Channel 28-Bit Inductance to Digital Converter (LDC) for Inductive Sensing*, Texas Instruments, https://www.ti.com/product/LDC1612, 2018.

[13] F. Tokgoz, G. Cakal, and O. Keysan, "Comparison of pcb winding topologies for axial-flux permanent magnet synchronous machines," *IET Electric Power Applications*, vol. 14, 02 2021.